Letter

Effects of higher-order Casimir-Polder interactions on Rydberg atom spectroscopy

B. Dutta, J. C. de Aquino Carvalho, G. Garcia-Arellano, P. Pedri, and A. Laliotis*
Laboratoire de Physique des Lasers, Université Sorbonne Paris Nord, F-93430 Villetaneuse, France and CNRS, UMR 7538, LPL, 99 Avenue J.-B. Clément, F-93430 Villetaneuse, France

C. Boldt, J. Kaushal, and S. Scheel†
Institute for Physics, University of Rostock, Albert-Einstein-Straße 23-24, D-18059 Rostock, Germany

(Received 15 January 2024; accepted 12 March 2024; published 9 May 2024)

In the extreme near field, when the spatial extension of the atomic wavefunction is no longer negligible compared to the atom-surface distance, the dipole approximation is no longer sufficient to describe Casimir-Polder interactions. Here we calculate the higher-order, quadrupole and octupole, contributions to Casimir-Polder energy shifts of Rydberg atoms close to a dielectric surface. We subsequently investigate the effects of these higher-order terms in thin-cell and selective reflection spectroscopy. Beyond its fundamental interest, this regime of extremely small atom surface separations is relevant for quantum technology applications with Rydberg or surface-bound atoms interfacing with photonic platforms.

DOI: 10.1103/PhysRevResearch.6.L022035

Highly excited (Rydberg) atoms have huge electric and magnetic transition multipole moments that make them interact very strongly with their environment. Thus, they are ideal candidates for studying dispersion forces such as Casimir-Polder (atom-surface) [1,2] or van der Waals (atom-atom) interactions [3]. More recently, Rydberg atoms have attracted significant attention for quantum technology applications. In particular, it was demonstrated that probing Rydberg atoms inside thin vapor cells [4] presents a simple way to fabricate room-temperature single-photon sources based on the Rydberg blockade effect [5], without having to resort to complex cold atom manipulations. Moreover, Rydberg atoms in vapor cells are being used as electric-field probes at THz or GHz frequencies [6–8]. However, the rapid scaling of electric-dipole moment fluctuations makes Casimir-Polder (CP) interactions a dominant spectroscopic contribution that impacts potential hybrid systems such as tapered optical fibers [9,10], hollow core fibers [11], and thin cells [4,5] that aim at interfacing atoms with photonic platforms. Similarly, Rydberg interactions with van der Waals heterostructures have also been investigated [12].

Theoretical studies of the interaction between dielectric surfaces and highly excited atoms have exposed the limitations of the traditional Casimir-Polder (CP) approach in which only the electric dipole interaction is taken into account. Indeed, the dipole approximation breaks down and higher-order terms need to be considered in the extreme near field [13] as Rydberg wavefunctions can easily extend beyond 100 nm (being proportional to $n^{\star 2}$, with $n^\star$ the effective quantum number). Moreover, perturbative approaches have also been questioned when the expected energy shifts are comparable to adjacent energy level spacings [14]. Although previous theoretical studies have presented the basic scaling laws governing quadrupole interactions [13], detailed results of the higher-order interaction coefficients have not yet been presented for CP atom-surface interactions. Higher-order effects have nevertheless been studied in detail for the case of atom-atom or molecule-molecule van der Waals interactions [15,16].

Atom-surface experiments have similarly flourished during the past decades [17–20], shedding light on novel effects such as the temperature dependence of CP interactions [19,21], and atom-metamaterial interactions [22] with an ever increasing precision in view of uncovering fundamental forces beyond the standard model [20]. However, higher-order interactions remain so far experimentally unexplored. A prominent and well-developed experimental method for performing such studies is vapor cell spectroscopy [21,23–26]. Thin vapor cells allow for a controlled confinement of atomic vapors within dielectric walls down to the nanometer regime, making them excellent platforms for probing Rydberg atoms extremely close to dielectric surfaces [4,25]. Selective reflection in macroscopic cells has also been used for atomic or molecular gases [21,23,27] close to a surface, but provides no means of controlling the probing depth, typically defined by the excitation wavelength.

Here, we investigate higher-order (quadrupole and octupole) CP interactions between a Rydberg atom and a dielectric surface, providing explicit calculations of the C_3 (dipole-dipole) and the C_5 (combined quadrupole-quadrupole and dipole-octupole) coefficients for alkali Rydberg atoms in the near field. We subsequently study the effects of higher-order interactions on CP vapor cell spectroscopy, illuminating the conditions under which higher-order interactions can be

*laliotis@univ-paris13.fr
†stefan.scheel@uni-rostock.de

experimentally measurable. Multipole contributions are of importance for experiments aiming at binding atoms to surfaces and extending the optical control to the extreme near field [28].

We will conduct our studies in the electrostatic limit, where CP Rydberg-surface interactions can be described as the interaction of the atomic charge distribution (centred in O) with its surface-induced instantaneous image (centred in O') in front of a perfectly conducting surface. We assume that the Rydberg atom consists of a valence electron orbiting around a positively charged core. The atom-surface interaction energy W is half the electrostatic energy of the atomic charge distribution placed under the external potential of its image $\Phi'(\vec{r}')$ with the corresponding field $\vec{E}'(\vec{r}')$,

$$W = -\frac{1}{2}\vec{p}\cdot\vec{E}'(\vec{r}_0) - \frac{1}{12}\sum_{i,j} Q_{ij}\frac{\partial E'_i}{\partial r'_j}(\vec{r}_0) - \frac{1}{24}\sum_{i,j,k} T_{ijk}\frac{\partial^2 E'_i}{\partial r'_j \partial r'_k}(\vec{r}_0) + \dots \quad (1)$$

Here, $\vec{r}_0$ is the position vector of the atom with coordinates r_i. The atomic multipole moments with respect to O are denoted as $\vec{p}$, $\bar{Q}$, and $\overline{\overline{T}}$ (dipole, quadrupole, and octupole moments, respectively). The potential created by the image can itself be expanded into multipoles, giving

$$\Phi'(\vec{r}_0) = \frac{1}{4\pi\epsilon_0}\sum_i p'_i\frac{r_{0i}}{r_0^3} + \frac{1}{8\pi\epsilon_0}\sum_{i,j} Q'_{ij}\frac{r_{0i}r_{0j}}{r_0^5} + \frac{1}{24\pi\epsilon_0}\sum_{i,j,k} T'_{ijk}\frac{r_{0i}r_{0j}r_{0k}}{r_0^7} + \dots \quad (2)$$

Here, $\vec{p}'$, $\bar{Q}'$, and $\overline{\overline{T}}'$ are the dipole, quadrupole, and octupole moments of the image with respect to O'. Symmetry links the components of the image moments to those of the atomic moments by $p'_i = (-1)^{\kappa+1}p_i$, $Q'_{ij} = (-1)^{\kappa+1}Q_{ij}$, $T'_{ijk} = (-1)^{\kappa+1}T_{ijk}$, where κ is the number of times z appears as a tensor index.

The CP interaction energy can therefore be written as

$$W = W_{pp} + W_{pQ} + W_{QQ} + W_{pT}, \quad (3)$$

where W_{pp}, W_{pQ}, W_{QQ}, W_{pT} are the dipole-dipole, dipole-quadrupole, quadrupole- quadrupole, and dipole-octupole contributions, respectively. The dipole-dipole and quadrupole-quadrupole terms are given by

$$W_{pp} = -\frac{1}{4\pi\epsilon_0}\frac{p^2 + p_z^2}{16 z_s^3}, \quad (4)$$

$$W_{QQ} = -\frac{17Q_{zz}^2 + 16Q_{zy}^2 + 16Q_{zx}^2 + 2Q_{xx}^2 + 4Q_{yx}^2 + 2Q_{yy}^2}{4\pi\epsilon_0 768 z_s^5}. \quad (5)$$

The cross terms such as the dipole-quadrupole and dipole-octupole contributions with their z_s^{-4} and z_s^{-5} dependence, respectively, are given in the Supplemental Material [30]. It should be noted that W_{pQ} includes both the energy of a dipole immersed in the field of a quadrupole and vice-versa (the same applies to W_{pT}).

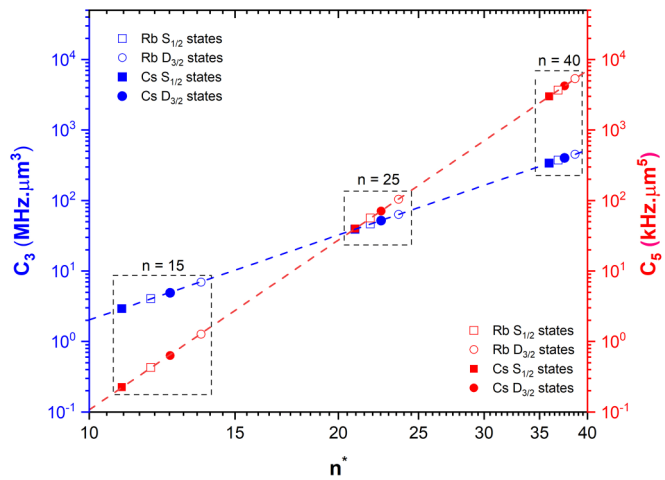

FIG. 1. C_3 and C_5 coefficients (blue and red colors, respectively) for $S_{1/2}$ and $D_{3/2}$ states (squares and circles, respectively) of cesium and rubidium (open and closed points, respectively) as a function of the effective quantum number $n^\star = n - \delta$. The straight-solid lines correspond to the analytical expressions derived for a hydrogen S state [Eqs. (7) and (8)] providing an accurate estimate, to within 1%, of the interaction coefficients for all alkali Rydberg atoms.

In the electrostatic limit, we can calculate the CP frequency shift Δf of an atomic Rydberg state using first-order perturbation theory as

$$h\Delta f = \langle\psi_{n,l,J,M_J}|W|\psi_{n,l,J,M_J}\rangle. \quad (6)$$

Here, ψ_{n,l,J,M_J} is the wavefunction of the Rydberg electron, with n the principal quantum number, l, J the orbital and total angular momentum quantum numbers, and M_J the projection of J onto the z axis. For Rydberg atoms we can assume that the external electron is under the influence of a central potential given by an effective Coulomb interaction modified to include the polarizability of core electrons [29]. This allows us to easily obtain the radial wavefunction by numerically solving Schrödinger's equation using the Numerov method. In our analysis, we ignore the hyperfine structure of the atoms as it is usually very small compared to the CP energy shifts for most alkali Rydberg atoms. The above analysis allows us to calculate Rydberg-surface interactions at any multipole order.

The quantum mechanical averaging of the interaction energy gives the following results: (a) The dipole-dipole term (Δf_3) yields the well-known near-field Casimir-Polder frequency shift $\Delta f_3 = -C_3/z_s^3$, where C_3 is a coefficient usually expressed in MHz µm^3. (b) The dipole-quadrupole terms vanish for parity reasons. (c) The quadrupole-quadrupole and dipole-octupole terms give a frequency shift expressed as $\Delta f_5 = -C_5/z_s^5$, where C_5 is a coefficient expressed in MHz µm^5. We emphasize that the dipole-octupole contributions do not necessarily vanish as both dipole and octupole interactions can act on the same atomic transition ($\Delta l = \pm 1$ transitions can be both dipole and octupole allowed). However, dipole-octupole terms only contribute to the anisotropy of the atom-surface interaction, with an overall scalar component (averaging over all M_J) that remains zero.

In Fig. 1 we plot the C_3 and C_5 coefficients for $S_{1/2}$ and $D_{3/2}$ states of cesium and rubidium atoms as a function of the

effective quantum number ($n^* = n - \delta^*$), where δ^* is the quantum defect. It shows that the interaction coefficients depend very little on the core polarizability and on angular momentum. We have therefore calculated analytical expressions for both C_3 and C_5 coefficients for a hydrogen atom. For an $S_{1/2}$ state ($l = 0$) the interaction coefficients become

$$C_3 = \frac{e^2 a_o^2}{96\pi\epsilon_0 h} n^{\star 2}(5n^{\star 2} + 1) \approx \frac{5e^2 a_o^2 n^{\star 4}}{96\pi\epsilon_0 h}, \tag{7}$$

$$C_5 = \frac{e^2 a_o^4}{640\pi\epsilon_0 h} n^{\star 4}(63n^{\star 4} + 105n^{\star 2} + 12) \approx \frac{63e^2 a_o^4 n^{\star 8}}{640\pi\epsilon_0 h}. \tag{8}$$

The full solution, for all states, is given in the Supplemental Material [30]. Recall that for hydrogen $n^\star$ is simply the principal quantum number and note that the leading term in the above polynomials is independent of angular momentum.

Our assumption of a perfectly correlated image breaks down at distances comparable to relevant transition wavelengths or when a frequency-dependent dielectric constant is considered [31]. However, for Rydberg atoms, the relevant multipole transitions are typically in the THz or GHz regime suggesting that retardation can be ignored at micrometer distances. Moreover, at these frequencies most materials do not possess surface resonances, and their dielectric constant tends to their static (ϵ_s) value. Dielectric effects can therefore be accounted for by simply multiplying the dispersion coefficients (Fig. 1) by the surface response ($S = \frac{\epsilon_s - 1}{\epsilon_s + 1}$), while temperature effects [21,32,33] are negligible and can be ignored [34]. The above arguments suggest that the electrostatic limit is a good approximation for studying Rydberg-surface interactions in the extreme near field. However, a QED treatment [35–37] would be necessary for treating the coupling of atoms with resonant surfaces or metasurfaces.

At this point, a word of caution is appropriate. Frequently, traceless multipole tensors are used in the calculation. However, this is only justified for quadrupole tensors, as its trace component does not contribute to the energy. This is no longer true for the octupole tensor, where the trace does in general contribute to the energy [38,39]. Indeed, upon reducing the quantity $r_i r_j r_k$ appearing in $\overline{\overline{T}}$ in terms of spherical harmonics yields terms with $Y_{3m}(\Theta, \varphi)$ (traceless part) as well as $Y_{1m}(\Theta, \varphi)$ (trace part). The latter can be identified as a contribution to the dipole transition, and only further symmetry considerations of the field distribution or atomic transition matrix elements can cause them to vanish [40,41].

Having developed a theoretical framework that allows us to calculate both C_3 and C_5 coefficients, we can estimate the effects of quadrupole interactions on CP experiments. Atomic spectroscopy in vapor cells of variable nanometric thickness (thin cells) is a well-developed method for measuring CP interactions with excited states including Rydberg atoms [25,42]. Thin cells allow us to control the vapor confinement down to the nanometer regime (thickness can be as small as 50 nm) [25], giving them a distinct advantage over other methods for probing higher-order CP interactions with Rydberg atoms.

Typically, a two-step excitation technique is used to reach high-lying excited states of alkali atoms [21,24,25]. For cesium (our atom of choice), a strong pump excites atoms to their first excited state ($6P_{1/2}$ or $6P_{3/2}$) and a weak laser probes the $6P_{1/2} \rightarrow$ nS or $6P_{1/2} \rightarrow$ nD transitions. For states with $n \approx 20$, the transition wavelength λ_{probe} is about 510 nm. In Fig. 2 we show the basic principle of the experiment that will be analyzed. Interatomic collisions and radiation trapping in the atomic vapor redistribute the initially velocity selected $6P$ population to many atomic velocities and hyperfine states. This allows us to consider our atoms essentially as two level systems in linear interaction with the probe excitation field. Thin cells form a low finesse Fabry-Perot cavity that eventually mixes the backward (reflection I_R^{lin}) and forward (transmission I_T^{lin}) response of the polarized atomic vapor [43] given by

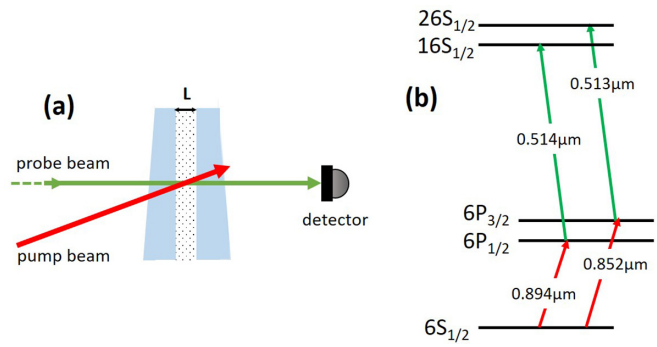

FIG. 2. (a) Schematic of the thin cell experiment analyzed in our simulations. A laser beam at 0.894 µm or 0.852 µm pumps cesium atoms to the $6P_{1/2}$ or $6P_{1/2}$ level, respectively. Subsequently, a green laser at 0.514 µm or 0.513 µm probes Rydberg atoms at the $6P_{1/2} \rightarrow 16S_{1/2}$ or the $6P_{3/2} \rightarrow 26S_{1/2}$ transition, respectively. Higher lying states can also be easily accessed via the same scheme. Because of interatomic collisions, the population of the intermediate levels has a quasithermal (Maxwell-Boltzmann) velocity distribution. (b) Relevant energy levels.

$$I_R^{\text{lin}} \propto \frac{N\mu^2}{\mathcal{F}} \int_0^\infty \frac{dv_z}{v_z} W(v_z) \int_0^L dz \int_0^z dz' e^{2ikz} e^{\frac{\mathcal{L}(z') - \mathcal{L}(z)}{v_z}}, \tag{9}$$

$$I_T^{\text{lin}} \propto \frac{N\mu^2}{\mathcal{F}} \int_0^\infty \frac{dv_z}{v_z} W(v_z) \int_0^L dz \int_0^z dz' e^{\frac{\mathcal{L}(z') - \mathcal{L}(z)}{v_z}}. \tag{10}$$

For a symmetric Fabry-Perot cavity with reflection coefficient r for both interfaces the transmission signal (S_T) that consists of the homodyne beating between the atomic response with that of an empty cavity is given by

$$S_T \propto \frac{2N\mu^2}{|\mathcal{F}|^2} \Re\left[I_T^{\text{lin}} + r^2 e^{2ikL} I_T^{\text{lin}} - 2r I_R^{\text{lin}}\right]. \tag{11}$$

Here, $\mathcal{F} = 1 - r^2 e^{2ikL}$ with r the reflection coefficient of the windows and $k = 2\pi/\lambda_{\text{probe}}$. The atomic velocity along the probe beam propagation axis is denoted as v_z, the atomic vapor density inside the cell is N and the transition dipole moment is μ. In the above equations, the functions $\mathcal{L}(z') - \mathcal{L}(z)$ are

$$\mathcal{L}(z') - \mathcal{L}(z) = \int_z^{z'} [\Gamma/2 - i(\delta + 2\pi\Delta f_{CP}(\xi) - kv_z)] d\xi,$$

where $\Delta f_{CP}(z)$ is the CP shift of the Rydberg state (the shift of the $6P$ state is negligible) inside the thin-cell cavity. The shift can be separated into a dipole component and a

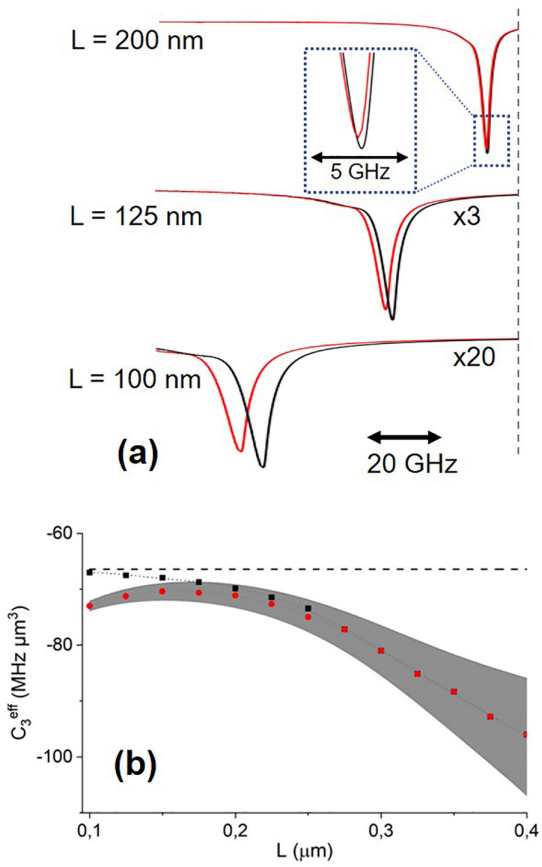

FIG. 3. (a) Thin-cell transmission spectra for three different thicknesses, calculated using Eq. (11) (S_T) with $C_3 = 4.15$ MHz µm^3 and C_5=0.45 kHz µm^5, corresponding to Cs $16S_{1/2}$ atoms. Dashed-vertical line: position of the transition frequency in the volume. Straight-red lines, calculations including both dipole and quadrupole interactions (C_3 and C_5). Black lines, dipole interactions only. The transmission amplitude decreases with thickness by a factor indicated in the figure. (b) Displacement of the transmission dip $C_3^{\rm eff}$ with respect to the volume transition frequency (dashed line), multiplied by L^3, as a function of cell thickness. Red dots, calculations with full CP potential. Black dots, dipole interactions only. Horizontal-dashed line, CP dipole shift in the center of the cell multiplied by L^3.

quadrupole component that depend on the C_3 and C_5 coefficients, respectively. As full calculation of the CP shift inside a cavity requires a more elaborate theory, we will not consider resonant effects due to surface polaritons and simply add the potentials of both walls, neglecting the infinite series of multiple images. In this case, the dipole and quadrupole shifts in the middle of the cell become $-16C_3/L^3$ and $-64C_5/L^5$, respectively.

In Fig. 3(a) we show the transmission spectrum of a resonant $6P_{1/2} \rightarrow 16S_{1/2}$ beam through a thin cell of three different thicknesses. The atom-surface interaction coefficients calculated for the $16S_{1/2}$ state of cesium (with a Bohr diameter of ≈15 nm) are $C_3 = 4.15$ MHz µm^3 and $C_5 = 0.45$ kHz µm^5. The red curves represent the calculated spectra using both dipole and quadrupole interactions, whereas for black curves the quadrupole interactions are omitted. The effect of quadrupole interactions becomes observable when the atomic vapor is confined at thicknesses smaller than 20 nm. At L = 100 nm the additional quadrupole shift exceeds the predicted spectral width, suggesting that the C_5 coefficient could be measurable with a thin-cell spectroscopy experiment. Figure 3(b) shows the predicted displacement of the transmission dip $C_3^{\rm eff}$ with respect to the volume resonance away from the surface, multiplied by L^3. When quadrupole interactions are ignored (black dots), $C_3^{\rm eff}$ tends towards $16C_3$ (dashed-horizontal line), suggesting that when the cell is very thin, the dominant spectral contribution derives from atoms at the center of the cell. For increasing cell thicknesses, the contribution of layers closer to the walls becomes more prominent leading to a larger $C_3^{\rm eff}$. Red dots represent calculations including both dipole and quadrupole interactions. From Fig. 3(b) we can see that quadrupole interactions have no visible effect for thicknesses larger than 250 nm. The extent of the gray-shaded area is $L^3w/5$, where w is the width of the transmission spectrum. The gray shaded area gives an indication of the capability of the proposed experiment to discern between the two models (black and red dots). Note that the discerning capability also depends on the signal to noise ratio of the experiment. The reduction in signal amplitude is noted in Fig. 3(a) next to the transmission curves. The effects of higher-order interactions are evident for larger cell thicknesses when probing higher-lying states such as $28S_{3/2}$ via the $6P_{1/2} \rightarrow 28S_{3/2}$ transition (see Supplemental Material [30].

Our above analysis assumes that Rydberg atoms interact with surfaces only via CP interactions. However, Stark shifts due to adsorbed atoms or parasitic electric field in the surface of the dielectric windows are known to be an important problem in precision atom-surface experiments [20,44–46]. In particular, high-lying states become extremely sensitive to electric fields [4,47] as their polarizability scales more rapidly ($\alpha \propto n^{\star 7}$) than the C_3 coefficient. Our analysis suggests that higher-order CP effects can be measurable even with relatively low-lying Rydberg states with $n^\star \approx 10\ldots15$, for which atom-surface interaction experiments have already been demonstrated [1,2]. This is a powerful indication that vapor cell spectroscopic experiments could provide excellent testbeds for further exploring Casimir-Polder physics.

We acknowledge insightful discussions with M. Ducloy and discussions with I. Maurin on the numerical modeling of thin cell spectra. This work was financially supported by the ANR-DFG grant SQUAT (Grants No. ANR-20-CE92-0006 and No. DFG SCHE 612/12-1), the DAAD and Campus France (via the PHC-PROCOPE Programme, Grant No. 57513024), and the French Embassy in Germany (via the Campus-France PHC-Procope Project No. 44711VG and via PROCOPE Mobilité, Project No. DEU-22-0004 LG1).

[1] V. Sandoghdar, C. I. Sukenik, E. A. Hinds, and S. Haroche, Direct measurement of the van der Waals interaction between an atom and its images in a micron-sized cavity, Phys. Rev. Lett. **68**, 3432 (1992).

[2] V. Sandoghdar, C. I. Sukenik, S. Haroche, and E. A. Hinds, Spectroscopy of atoms confined to the single node of a standing wave in a parallel-plate cavity, Phys. Rev. A **53**, 1919 (1996).

[3] L. Béguin, A. Vernier, R. Chicireanu, T. Lahaye, and A. Browaeys, Direct measurement of the van der Waals interaction between two Rydberg atoms, Phys. Rev. Lett. **110**, 263201 (2013).

[4] H. Kübler, J. P. Shaffer, T. Baluktsian, R. Löw, and T. Pfau, Coherent excitation of Rydberg atoms in micrometre-sized atomic vapour cells, Nat. Photon. **4**, 112 (2010).

[5] F. Ripka, H. Kübler, R. Löw, and T. Pfau, A room-temperature single-photon source based on strongly interacting Rydberg atoms, Science **362**, 446 (2018).

[6] J. A. Sedlacek, A. Schwettmann, H. Kübler, R. Löw, T. Pfau, and J. P. Shaffer, Microwave electrometry with Rydberg atoms in a vapour cell using bright atomic resonances, Nat. Phys. **8**, 819 (2012).

[7] C. G. Wade, N. ibali, N. R. De Melo, J. M. Kondo, C. S. Adams, and K. J. Weatherill, Real-time near-field terahertz imaging with atomic optical fluorescence, Nat. Photon. **11**, 40 (2017).

[8] L. A. Downes, A. R. MacKellar, D. J. Whiting, C. Bourgenot, C. S. Adams, and K. J. Weatherill, Full-field terahertz imaging at kilohertz frame rates using atomic vapor, Phys. Rev. X **10**, 011027 (2020).

[9] K. S. Rajasree, T. Ray, K. Karlsson, J. L. Everett, and S. N. Chormaic, Generation of cold Rydberg atoms at submicron distances from an optical nanofiber, Phys. Rev. Res. **2**, 012038 (2020).

[10] A. Vylegzhanin, D. J. Brown, A. Raj, D. F. Kornovan, J. L. Everett, E. Brion, J. Robert, and S. N. Chormaic, Excitation of ^{87}Rb Rydberg atoms to nS and nD states ($n \leqslant 68$) via an optical nanofiber, arXiv:2305.05186.

[11] G. Epple, K. S. Kleinbach, T. G. Euser, N. Y. Joly, T. Pfau, P. S. J. Russell, and R. Löw, Rydberg atoms in hollow-core photonic crystal fibres, Nat. Commun. **5**, 4132 (2014).

[12] K. Wongcharoenbhorn, C. Koller, T. M. Fromhold, and W. Li, Casimir-Polder interactions of *s*-state Rydberg atoms with graphene, Phys. Rev. A **107**, 043308 (2023).

[13] J. A. Crosse, S. A. Ellingsen, K. Clements, S. Y. Buhmann, and S. Scheel, Thermal Casimir-Polder shifts in Rydberg atoms near metallic surfaces, Phys. Rev. A **82**, 010901(R) (2010).

[14] S. Ribeiro, S. Y. Buhmann, T. Stielow, and S. Scheel, Casimir-polder interaction from exact diagonalization and surface-induced state mixing, Europhys. Lett. **110**, 51003 (2015).

[15] J. K. Jenkins, A. Salam, and T. Thirunamachandran, Retarded dispersion interaction energies between chiral molecules, Phys. Rev. A **50**, 4767 (1994).

[16] A. Salam and T. Thirunamachandran, A new generalization of the Casimir-Polder potential to higher electric multipole polarizabilities, J. Chem. Phys. **104**, 5094 (1996).

[17] H. Bender, P. W. Courteille, C. Marzok, C. Zimmermann, and S. Slama, Direct measurement of intermediate-range Casimir-Polder potentials, Phys. Rev. Lett. **104**, 083201 (2010).

[18] J. C. de Aquino Carvalho, I. Maurin, P. Chaves de Souza Segundo, A. Laliotis, D. de Sousa Meneses, and D. Bloch, Spectrally sharp near-field thermal emission: Revealing some disagreements between a Casimir-Polder sensor and predictions from far-field emittance, Phys. Rev. Lett. **131**, 143801 (2023).

[19] J. M. Obrecht, R. J. Wild, M. Antezza, L. P. Pitaevskii, S. Stringari, and E. A. Cornell, Measurement of the temperature dependence of the Casimir-Polder force, Phys. Rev. Lett. **98**, 063201 (2007).

[20] M. Antezza, L. P. Pitaevskii, and S. Stringari, Effect of the Casimir-Polder force on the collective oscillations of a trapped Bose-Einstein condensate, Phys. Rev. A **70**, 053619 (2004).

[21] A. Laliotis, T. Passerat de Silans, I. Maurin, M. Ducloy, and D. Bloch, Casimir-Polder interactions in the presence of thermally excited surface modes, Nat. Commun. **5**, 4364 (2014).

[22] E. A. Chan, S. A. Aljunid, G. Adamo, A. Laliotis, M. Ducloy, and D. Wilkowski, Tailoring optical metamaterials to tune the atom-surface Casimir-Polder interaction, Sci. Adv. **4**, eaao4223 (2018).

[23] M. Oria, M. Chevrollier, D. Bloch, M. Fichet, and M. Ducloy, Spectral observation of surface-induced van der Waals attraction on atomic vapour, Europhys. Lett. **14**, 527 (1991).

[24] H. Failache, S. Saltiel, M. Fichet, D. Bloch, and M. Ducloy, Resonant van der Waals repulsion between excited Cs atoms and sapphire surface, Phys. Rev. Lett. **83**, 5467 (1999).

[25] M. Fichet, G. Dutier, A. Yarovitsky, P. Todorov, I. Hamdi, I. Maurin, S. Saltiel, D. Sarkisyan, M.-P. Gorza, D. Bloch, and M. Ducloy, Exploring the van der Waals atom-surface attraction in the nanometric range, Europhys. Lett. **77**, 54001 (2007).

[26] T. Peyrot, N. Šibalić, Y. R. P. Sortais, A. Browaeys, A. Sargsyan, D. Sarkisyan, I. G. Hughes, and C. S. Adams, Measurement of the atom-surface van der Waals interaction by transmission spectroscopy in a wedged nanocell, Phys. Rev. A **100**, 022503 (2019).

[27] J. Lukusa Mudiayi, I. Maurin, T. Mashimo, J. C. de Aquino Carvalho, D. Bloch, S. K. Tokunaga, B. Darquié, and A. Laliotis, Linear probing of molecules at micrometric distances from a surface with sub-doppler frequency resolution, Phys. Rev. Lett. **127**, 043201 (2021).

[28] D. Hümmer, O. Romero-Isart, A. Rauschenbeutel, and P. Schneeweiss, Probing surface-bound atoms with quantum nanophotonics, Phys. Rev. Lett. **126**, 163601 (2021).

[29] A. Derevianko, W. R. Johnson, M. S. Safronova, and J. F. Babb, High-precision calculations of dispersion coefficients, static dipole polarizabilities, and atom-wall interaction constants for alkali-metal atoms, Phys. Rev. Lett. **82**, 3589 (1999).

[30] See Supplemental Material at http://link.aps.org/supplemental/10.1103/PhysRevResearch.6.L022035 for details on the calculation of higher order Casimir-Polder interactions and on our numerical calculation of thin-cell spectra.

[31] M. Fichet, F. Schuller, D. Bloch, and M. Ducloy, van der Waals interactions between excited-state atoms and dispersive dielectric surfaces, Phys. Rev. A **51**, 1553 (1995).

[32] M.-P. Gorza and M. Ducloy, Van der Waals interactions between atoms and dispersive surfaces at finite temperature, Eur. Phys. J. D **40**, 343 (2006).

[33] G. Barton, van der Waals shifts in an atom near absorptive dielectric mirrors, Proc. R. Soc. London A **453**, 2461 (1997).

[34] A. Laliotis and M. Ducloy, Casimir-Polder effect with thermally excited surfaces, Phys. Rev. A **91**, 052506 (2015).

[35] H. B. G. Casimir and D. Polder, The influence of retardation on the London-van der Waals forces, Phys. Rev. **73**, 360 (1948).

[36] J. M. Wylie and J. E. Sipe, Quantum electrodynamics near an interface, Phys. Rev. A **30**, 1185 (1984).

[37] J. M. Wylie and J. E. Sipe, Quantum electrodynamics near an interface. II, Phys. Rev. A **32**, 2030 (1985).

[38] R. E. Raab, Magnetic multipole moments, Mol. Phys. **29**, 1323 (1975).

[39] R. E. Raab and O. L. de Lange, *Multipole Theory in Electromagnetism: Classical, Quantum, and Symmetry Aspects, with Applications* (Oxford University Press, Oxford, 2004).

[40] A. Salam, A general formula for the rate of resonant transfer of energy between two electric multipole moments of arbitrary order using molecular quantum electrodynamics, J. Chem. Phys. **122**, 044112 (2005).

[41] A. Salam, Corrections to the Casimir-polder potential arising from electric octupole coupling, Mol. Phys. **117**, 2217 (2019).

[42] B. Dutta, J. C. de Aquino Carvalho, G. G. Arellano, I. Maurin, D. Bloch, and A. Laliotis, Measuring the Casimir-Polder Rydberg-surface interaction by vapour cell spectroscopy, *25th International Conference of Spectral Line Shapes* (ICSL, Caserta, Italy, 2022).

[43] G. Dutier, S. Saltiel, D. Bloch, and M. Ducloy, Revisiting optical spectroscopy in a thin vapor cell: Mixing of reflection and transmission as a Fabry–Perot microcavity effect, J. Opt. Soc. Am. B **20**, 793 (2003).

[44] J. M. McGuirk, D. M. Harber, J. M. Obrecht, and E. A. Cornell, Alkali-metal adsorbate polarization on conducting and insulating surfaces probed with Bose-Einstein condensates, Phys. Rev. A **69**, 062905 (2004).

[45] J. M. Obrecht, R. J. Wild, and E. A. Cornell, Measuring electric fields from surface contaminants with neutral atoms, Phys. Rev. A **75**, 062903 (2007).

[46] Y. Balland, L. Absil, and F. P. dos Santos, Quectonewton local force sensor, arXiv:2310.14717.

[47] H. Hattermann, M. Mack, F. Karlewski, F. Jessen, D. Cano, and J. Fortágh, Detrimental adsorbate fields in experiments with cold Rydberg gases near surfaces, Phys. Rev. A **86**, 022511 (2012).